Shell evolution at $N = 20$ in the constrained relativistic mean field approach*

SUN Bao-Hua(孙保华)[1)] LI Jian(李剑)

(School of Physics and State Key Laboratory of Nuclear Physics and Technology, Peking University, Beijing 100871, China)

Abstract The shell evolution at $N = 20$, a disappearing neutron magic number observed experimentally in very neutron-rich nuclides, is investigated in the constrained relativistic mean field (RMF) theory. The trend of the shell closure observed experimentally towards the neutron drip-line can be reproduced. The predicted two-neutron separation energies, neutron shell gap energies and deformation parameters of ground states are shown as well. These results are compared with the recent Hartree-Fock-Bogliubov (HFB-14) model and the available experimental data. The perspective towards a better understanding of the shell evolution is discussed.

Key words shell quenching, $N = 20$, relativistic mean field theory, nuclear deformation

PACS 21.10.Dr, 21.60.Jz

1 Introduction

The occurrence of the magic numbers 2, 8, 20, 28, 50, 82 and 126 in the nuclear system at or close to the valley of stability has been one of the strongest motivations for the theoretical nuclear mean-field theories[1]. At these proton or neutron numbers, effects analogous to electron shell closures in atoms are observed. In order to reproduce this observed shell effect, a strong spin-orbit interaction (ls force) was introduced in the framework of a non-relativistic nuclear model by referring to the example from the atomic physics. However, how to incorporate the isospin dependence of the ls force is still an open problem such as to describe nuclides close to and far away from the beta stability simultaneously. On the other hand, within the relativistic model, the spin-orbit interaction is incorporated automatically in its equations. The central potential and the ls potential are inter-related through the scalar and the vector potentials. Therefore, in this aspect the relativistic model is a more basic model for understanding the ls force (thus shell closure) as well as its isospin dependence. However, since all nuclear models were constructed based on known experimental data near the valley of stability, it is a great challenge to predict also how and where the shell closures vary.

Recently, the breakdown of the neutron magic number $N = 20$ in the neutron-rich nuclei has been the subject of intense experimental and theoretical scrutiny. The precise mass measurements[2] and/or the observations of low-lying first excited states with large B(E2) transition probabilities (see, e.g. Ref. [3] and references therein) confirm a vanishing $N = 20$ shell gap for isotopes from O to Mg towards the neutron drip-line. Similarly, the traditional shell closures at $N = 8$ and 28 have been found to be disappearing with isospin in various experiments[4, 5], while on the other hand new shell closures like that at $N = 16$[4] appear. This reflects the ordering of the single-particle levels and thus the shell structure change with isospin. In the language of shell-model (see e.g., Ref. [6]), the structural changes around ^{32}Mg can be explained by the reason that the p-f configurations drop below the s-d ones. As illustrated in Fig. 1, this region around $N = 20$ sometimes is also refereed to as the "island of inversion".

The main purpose of this investigation is to explore the shell evolution towards the neutron drip-line in the framework of the relativistic mean field (RMF) approach by taking the $N = 20$ isotonic chain as an example, and to find the discrepancy between the

Received 25 April 2008

* Supported by Major State Basic Research Developing Program (2007CB815000), and National Natural Science Foundation of China (10435010, 10775004, 10221003)

1) E-mail: bhsunpku@gmail.com

theoretical predictions and the experimental results. In Section 2 a brief summary of the constrained RMF theory is given. In Section 3 the results are presented together with the comparisons with the experimental data and the predictions of the recent Hartree-Fock-Bogliubov (HFB-14) model[7]. Finally, the summary is given in the last section.

2 Constrained relativistic mean field approach

In the RMF approach, the nucleons interact via the exchange of mesons (σ, ω and ρ) and photons. The corresponding large scalar and vector fields, of the order of a few hundred MeV, provide simple and efficient descriptions of several important phenomena like the spin-orbital interaction and the pseudospin symmetry (for a recent review, see Refs. [8—12]).

The standard effective Lagrangian density of the RMF theory is constructed with the degrees of freedom associated with the nucleon field ψ, two isoscalar meson fields σ and ω, the isovector meson field ρ, and the photon field A:

$$\begin{aligned}\mathcal{L} = & \overline{\psi}[\mathrm{i}\gamma^{\mu}\partial_{\mu}-M]\psi-\overline{\psi}\Big[g_{\sigma}\sigma+ \\ & g_{\omega}\gamma^{\mu}\omega_{\mu}+g_{\rho}\gamma^{\mu}\boldsymbol{\tau}\cdot\boldsymbol{\rho}_{\mu}+e\gamma^{\mu}\frac{1-\tau_3}{2}A_{\mu}\Big]\psi+ \\ & \frac{1}{2}\partial^{\mu}\sigma\partial_{\mu}\sigma-\frac{1}{2}m_{\sigma}^2\sigma^2-\frac{1}{3}g_2\sigma^3-\frac{1}{4}g_3\sigma^4- \\ & \frac{1}{4}\omega^{\mu\nu}\omega_{\mu\nu}+\frac{1}{2}m_{\omega}^2\omega^{\mu}\omega_{\mu}+\frac{1}{4}c_3\left(\omega^{\mu}\omega_{\mu}\right)^2- \\ & \frac{1}{4}\boldsymbol{\rho}^{\mu\nu}\cdot\boldsymbol{\rho}_{\mu\nu}+\frac{1}{2}m_{\rho}^2\boldsymbol{\rho}^{\mu}\cdot\boldsymbol{\rho}_{\mu}+\frac{1}{4}d_3(\boldsymbol{\rho}^{\mu}\cdot\boldsymbol{\rho}_{\mu})^2- \\ & \frac{1}{4}A^{\mu\nu}A_{\mu\nu}\,, \end{aligned} \tag{1}$$

where all the symbols have the same meaning as in Ref. [13]. The corresponding Dirac equation for nucleons and Klein-Gordon equations for mesons obtained with the mean field approximation are solved by the expansion method in the widely used axially deformed Harmonic-Oscillator basis[12, 14]. The equation of motion for the photon field is solved using the standard Green's function method due to its long range. The number of shells used for expansion is chosen as $N_{\mathrm{f}}=N_{\mathrm{b}}=14$. The parameter set PK1[13] is used throughout the calculation. Contrary to a widely used phenomenological center-of-mass correction such as $-\frac{3}{4}41A^{-1/3}$, the center-of-mass correction is taken into account microscopically by

$$E_{\mathrm{cm}}^{\mathrm{mic}}=\frac{1}{2mA}\langle\boldsymbol{p}_{\mathrm{cm}}^2\rangle, \tag{2}$$

where $\boldsymbol{p}_{\mathrm{c.m.}}$ is the total momentum of a nucleus with A nucleons.

The pairing energy is calculated via the BCS method, where the proton and neutron pairing strengths G are optimized for each isotopic chain from Ne to Ti by fitting the experimental odd-even mass differences (four-point formula). Furthermore, in order to obtain the potential energy surfaces (PESs) and determine the corresponding deformation parameters of ground-states, quadrupole constrained calculations[1, 15] have been performed for all the nuclei investigated in this work.

3 Results and discussion

In the present work, all the even-even nuclides for elements from Ne to Ti with neutron number 18, 20 and 22 have been investigated in the RMF approach. These nuclides are illustrated in Fig. 1.

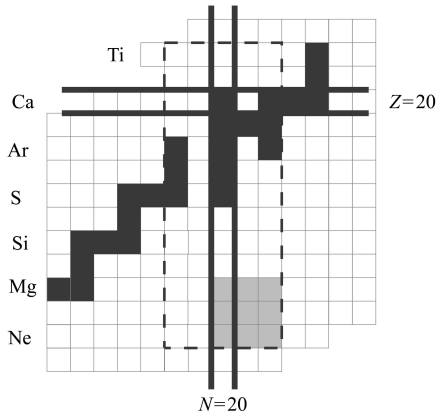

Fig. 1. Chart of nuclides around the island of inversion. Stable nuclei are shown in black squares. Magic proton and neutron numbers at $Z=20$ and $N=20$ are indicated by pairs of parallel lines. Even-even nuclides investigated in this work are in the region of the square marked by dashed lines. The island of inversion taken from Ref. [6] is shown as a grey area.

The two-neutron separation energy S_{2n} of nuclide (Z,N) is defined as

$$\begin{aligned}S_{2n}(Z,N) = & M(Z,N-2)+2M_n-M(Z,N)= \\ & E_{\mathrm{B}}(Z,N-2)-E_{\mathrm{B}}(Z,N)\,, \end{aligned} \tag{3}$$

where M_n, $M(Z,N)$ and $E_{\mathrm{B}}(Z,N)$, respectively, are the neutron mass, the nuclear mass and the binding energy for a nucleus (Z,N). It corresponds to the energy required to remove a pair of neutrons from a nucleus. As the first derivative of binding energies, two-neutron separation energies indicate the evolution of the binding energy with isospin. For an isotonic chain, the S_{2n} are getting steadily smaller with

the proton number Z. In Fig. 2, two-neutron separation energies from the experimental data[2] and the predictions of the RMF model for the isotonic chain with $N = 18$—24, are plotted as a function of proton number Z. Compared with the RMF calculation, the experimental results show kinks at nuclides with $Z = N$ due to the "so-called" Wigner effect. Since so far the Wiger effect has not been taken into account in the RMF approach, a much smooth relation of S_{2n} versus Z is observed. The RMF reproduces well the experimental values at the $N = 22$ and 24 chains, however, systematically overestimates the experimental results by about 2 MeV for the $N = 20$ chain with $Z = 10$—20.

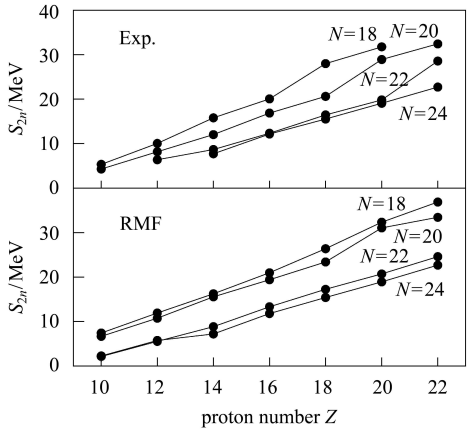

Fig. 2. Two-neutron separation energies (S_{2n}) for isotonic chains $N = 18$—22 as a function of proton number Z. The experimental data (upper panel) are taken from Ref. [2] and the theoretical results are calculated in the RMF approach.

The derivative of the two-nucleon separation energies, namely the shell gap energy defined as

$$\Delta_n(Z,N_0) = M(Z,N+2)-2M(Z,N)+ M(Z,N+2)= S_{2n}(Z,N_0)-S_{2n}(Z,N_0+2)\,, \quad (4)$$

is characterized by the vertical distance between two consecutive isotones. It is widely used to extract the shell strength from nuclear masses. The shell gap energy at $N = 20$ is plotted in Fig. 3 as a function of Z for the RMF predictions together with the experimental data[2] and the HFB-14[7] results. It is clear that both the theoretical calculations and the experimental data show the decline for the $N = 20$ shell gap approaching the drip-line. For the experimental data, the shell gap energies change from about 9 MeV at the double-magic nuclides ^{40}Ca to about 2.3 MeV at nuclides ^{30}Ne. The shell gap energy calculated in the RMF is about 2 MeV larger than the corresponding experimental value for the nuclides with $Z = 10$—18, and is about 1 MeV larger for ^{40}Ca. This is due to the predicted spherical ground state for nuclides with $N = 20$ in the RMF approach as shown in Fig. 4. The HFB-14 calculation shows a relatively better reproductive power for the shell gap, however, overestimates the shell quenching effect from ^{34}Si to ^{32}Mg by more than 3.5 MeV.

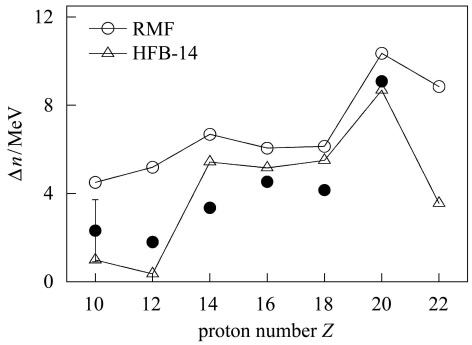

Fig. 3. Comparisons between the calculated neutron shell gaps at $N = 20$ in the RMF (open circles) and HFB-14[7] (open triangle) models with the experimental values[16] (filled circles).

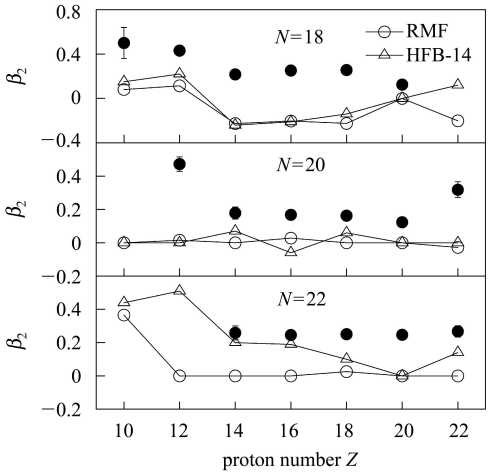

Fig. 4. The quadrupole deformation parameters β_2 of $N = 18$ (upper panel), 20 (middle panel) and 22 (lower panel) isotones as a function of proton number Z. The results from the RMF calculations (open circle) are compared with the experimental data[16] (filled circle) and those calculated from the HFB-14 model[7] (open triangle).

Experimental information[3, 16, 17] shows that the weakening of the $N = 20$ shell is related to the appearance of a deformed ground state. The corresponding deformation parameters obtained in the RMF and HFB-14 models are presented for isotonic chains with $N = 18$, 20 and 22 in Fig. 4. The available experimental data[16] are extracted from the $B(E2: 0^+ \to 2^+)$.

The RMF predictions are in very good agreement with the HFB-14 predictions for the $N = 18$ and 20

chains. The only difference for the $N=18$ chain is the ground state configuration for ^{40}Ti. In the HFB-14 model, a small prolate deformation $\beta_2=0.1$ is predicted. However, in our calculation the ground state is assigned to an oblate configuration with $\beta_2=-0.2$, while a second minimum of the energy surface with an excitation energy of 0.55 MeV is at a soft deformation of $\beta_2\approx 0.1$. As for the $N=20$ chain, both calculations fail to give the deformation of the ground state for ^{30}Ne[17] and ^{32}Mg[16]. In fact, this is a common problem of mean field theories as demonstrated also by the HFB-14 model. For this the angular momentum projection method[1, 11] can be introduced to restore the broken rotational symmetry. Furthermore, it has been demonstrated recently in Ref. [18] that the mean field picture of those nuclei is strongly modified by the projection. On the other hand, a relatively good reproductive power of the shell gap in the HFB-14 model probably is related to its global mass fit to all the known nuclear masses, thus some other effects compensate the effect due to wrongly assigned shapes of ground states. This is also a strong motivation for searching a Lagrangian parameter set suitable for the entire nuclear chart in the RMF approach, and this new parameter set is expected to incorporate the isospin dependence of e.g. pairing and shell closure.

Different from the agreement in predicting the ground state configurations for the $N=18$ and 20 chains, the HFB-14 and RMF models assign quite different shapes for the $N=22$ chain. From $Z=20$ to $Z=12$, a steadily increasing prolate deformation is predicted in the HFB-14 model, while a spherical shape is predicted in the RMF calculations. It is interesting to see whether the RMF theory can give the prolate shape as in the HFB-14. Fig. 5 presents the potential energy surface of ^{34}Mg as a function of the deformation parameter β_2. In the RMF approach, the ground state is spherical. The second minimum of the energy surface at $\beta_2=0.3$ is clearly seen and has an excitation energy of only 0.07 MeV, which may indicate a large probability of the shape coexistence for ^{34}Mg. Further investigations on the flat energy surface need to go beyond the mean field theory.

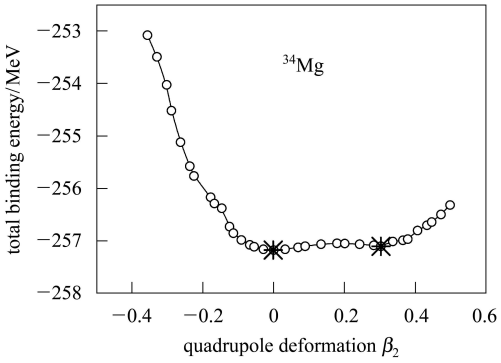

Fig. 5. The potential energy surfaces of ^{34}Mg as a function of the deformation parameter β_2. Two local minima have been marked.

4 Summary

In the present work, the RMF approach has been adopted to study the shell evolution towards the neutron drip-line at $N=20$. For each nuclide investigated, the quadrupole constrained calculations have been performed to obtain the ground state. It turned out that our calculation can reproduce the trend of the shell evolution towards the neutron drip-line, however, shows systematically larger shell gap energies by about 2 MeV compared with the experimental data. For a better understanding of the shell evolution, one needs to go beyond the mean field theory, e.g., introducing the angular momentum projection method.

The authors are indebted to Prof. Meng Jie for his valuable suggestions and critical review.

References

1 Ring P, Schuck P. The Nuclear Many-Body Problem. Berlin: Springer, 1980
2 Audi G, Wapstra A H, Thibault C. Nucl. Phys. A, 2003, **729**: 337
3 Penionzhkevich Yu E. Hyperfine Inter., 2006, **171**: 157
4 Ozawa A et al. Phys. Rev. Lett., 2000, **84**: 5493
5 Sarazin F et al. Phys. Rev. Lett., 2006, **84**: 5062
6 Warburton E K, Becker J A, Brown B A. Phys. Rev. C, 1990, **41**: 1147
7 Goriely S, Samyn M, Pearson J M. Phys. Rev. C, 2007, **75**: 064312
8 MENG J, Ring P. Phys. Rev. Lett., 1996, **77**: 3963
9 MENG J, Ring P. Phys. Rev. Lett., 1998, **80**: 460
10 ZHOU S G, MENG J, Ring P. Phys. Rev. Lett., 2003, **91**: 262501
11 Bender M, Heenen P H, Reinhard P G. Rev. Mod. Phys., 2003, **75**: 121
12 MENG J et al. Prog. Part. Nucl. Phys., 2006, **57**: 470
13 LONG W H et al. Phys. Rev. C, 2004, **69**: 034319
14 Gambhir Y K, Ring P, Thimet A. Ann. Phys. (NY), 1990, **194**: 132
15 Flocard H et al. Nucl. Phys. A, 1973, **203**: 433
16 Raman S et al. At. Data. Nucl. Data Tables, 2001, **78**: 1
17 Yanagisawa Y et al. Phys. Lett. B, 2003, **24**: 84
18 Robríguez-Guzmán R, Egido J L, Robledo L M. Phys. Lett. B, 2000, **474**: 15